ACS Medicinal Chemistry Letters

Letter

pubs.acs.org/acsmedchemlett

Discovery and Structure-Based Optimization of Adenain Inhibitors

Aengus Mac Sweeney,[†] Philipp Grosche,[†] David Ellis,[‡] Keith Combrink,[‡] Paul Erbel,[†] Nicola Hughes,[†] Finton Sirockin,[†] Samu Melkko,[†] Anna Bernardi,[†] Paul Ramage,[†] Nadine Jarousse,[§] and Eva Altmann*[,†]

[†]Novartis Institute for Biomedical Research, Novartis Campus, CH-4002 Basel, Switzerland

[‡]Novartis Institute for Biomedical Research, 6201 South Freeway, Fort Worth, Texas 76134-2099, United States

[§]Novartis Institute for Biomedical Research, 4560 Horton Street, Emeryville, California 94608-2916, United States

Supporting Information

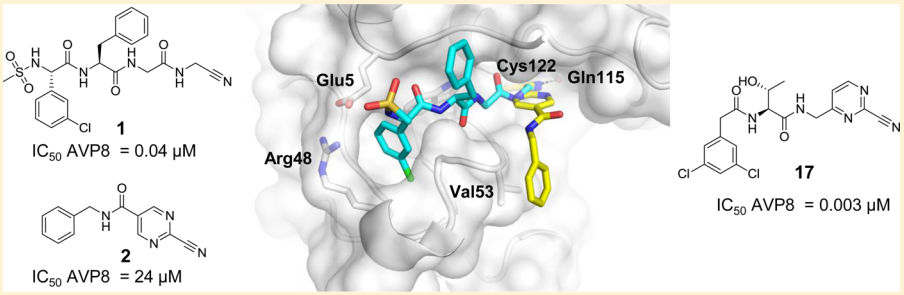

ABSTRACT: The cysteine protease adenain is the essential protease of adenovirus and, as such, represents a promising target for the treatment of ocular and other adenoviral infections. Through a concise two-pronged hit discovery approach we identified tetrapeptide nitrile **1** and pyrimidine nitrile **2** as complementary starting points for adenain inhibition. These hits enabled the first high-resolution X-ray cocrystal structures of adenain with inhibitors bound and revealed the binding mode of **1** and **2**. The screening hits were optimized by a structure-guided medicinal chemistry strategy into low nanomolar drug-like inhibitors of adenain.

KEYWORDS: *Adenoviral protease, adenoviral infection, inhibitor X-ray cocrystal structure, structure-based design*

Adenoviral infections are associated with several acute ocular, respiratory, and gastrointestinal pathologies.[1] Adenovirus disease in immunocompetent individuals is mostly self-limiting with few long-term implications.[2] However, epidemic keratoconjunctivitis (EKC), which is associated with serotypes 8, 37, and 64,[3,4] is a highly contagious adenoviral ocular infection with potential consequences for visual acuity.[5] To date, there are no specific therapies for adenoviral infections available. The cysteine protease adenain, the adenovirus protease,[6,7] is involved in several critical steps during virus propagation, including early and late stages of the replication cycle.[8] Adenain supports uncoating of the viral particles during viral entry,[9] it is responsible for processing several capsid and core precursor proteins required for the formation of mature, infectious virions, and it has also been implicated in host cell lysis through cleavage of cytoskeletal proteins.[10,11] Thus, the specific inhibition of adenain may offer an efficacious treatment strategy for adenoviral infections such as EKC.

As there are no low molecular weight (LMW) inhibitors of the active form of adenain described,[12] we used a two-pronged fast track hit discovery approach to identify starting points for medicinal chemistry. On one hand, we prepared a peptide array that mimicked the consensus substrate cleavage sites[13] of adenain, with iterative variations of the P4 and P3 amino acids and the incorporation of a nitrile moiety as an electrophilic warhead at the P1 subunit. This effort resulted in the identification of the highly potent tetrapeptide nitrile **1**. On the other hand, we performed a focused screen of selected heterocyclic nitriles, which yielded the weak, fragment-like pyrimidine nitrile **2** (Figure 1) as an alternative starting point for medicinal chemistry.

Importantly, we were able to obtain X-ray cocrystal structures of both hits in complex with adenain prior to the initiation of hit-to-lead activities. As illustrated in Figure 2 both inhibitors were found to be covalently bound to the catalytic Cys residue (Cys122) of adenain through their nitrile group. For tetrapeptide **1** (Figure 2A) the peptide chain expands into

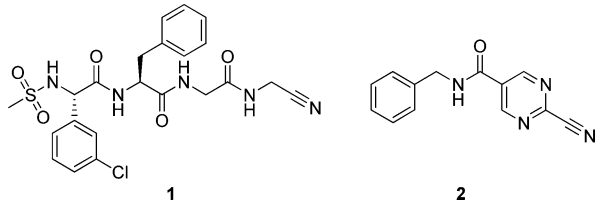

Figure 1. Structures of tetrapeptide nitrile hit **1**, IC_{50} = 0.04 μM, and pyrimidine nitrile hit **2**, IC_{50} = 24 μM.

Received: May 28, 2014
Accepted: June 20, 2014
Published: June 20, 2014

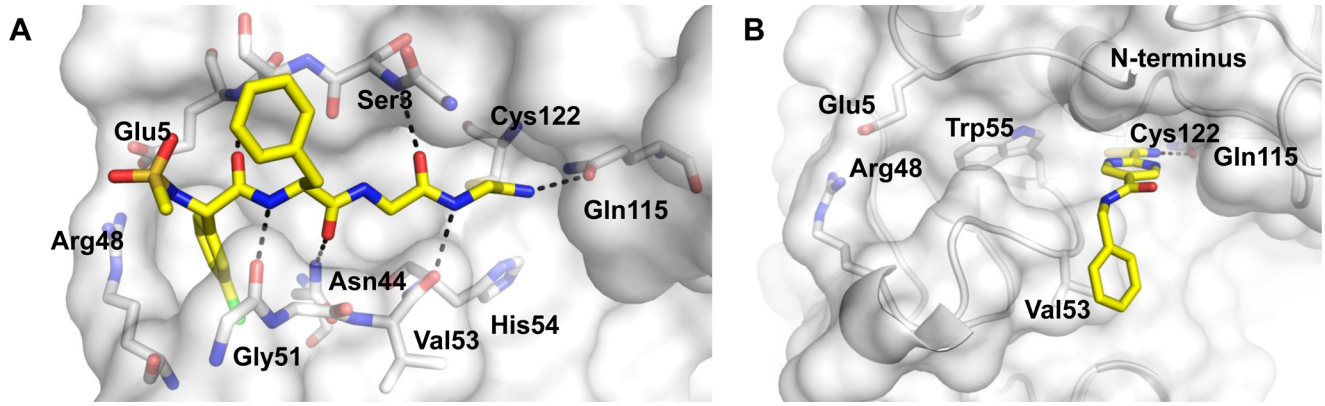

Figure 2. X-ray cocrystal structures: Inhibitor **1** bound in the active site of AVP2 (A, PDB code 4PIE) and inhibitor **2** bound in the active site of AVP2 (B, PDB code 4PID). The pictures were produced using PyMol.

Table 1. Exploring P4/P3 SAR for the Glycine Nitrile Series

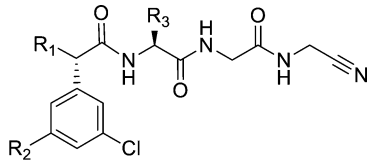

compd	R1	R2	R3	IC_{50} AVP8[a] (μM)	IC_{50} AVP5[a] (μM)	Caco-2 (A–B)/(B–A) (10^{-6} cm/s)	log Pampa (10^{-6} cm/s)	Sol[b] (μM)	PSA (Å^2)	MW[c]
1	CH_3SO_2NH	H	$C_6H_5CH_2$	0.04	0.03	1.2/7.5	−5.6	170	157	505
3	H	H	$C_6H_5CH_2$	0.38	0.28	1.2/7.4	−5.4	150	111	412
4	OH	H	$C_6H_5CH_2$	0.07	nd[d]	2.2/3.2	nd[d]	nd[d]	131	428
5	H	Cl	$C_6H_5CH_2$	0.07	0.04	1.2/8.1	−5.5	30	111	447
6	CH_3[e]	Cl	$C_6H_5CH_2$	0.03	0.006	nd[d]	−5.3	50	111	461
7	H	Cl	$C_5H_5NCH_2$[e]	0.36	0.14	0.7/15	−5.5	111	124	448
8	H	Cl	H_2NCH_2	0.08	0.04	1.0/1.2	−5.1	891	137	386
9	H	Cl	$CH_3CH(OH)$	0.08	0.03	nd[d]	−5.3	121	131	401
10	H	Cl	$(CH_3)_3C$	0.08	0.04	5.4/23.8	−5.4	85	111	413
11	OH	Cl	$CH_3CH_2CH(CH_3)$	0.05	0.05	3.0/28	nd[d]	nd[d]	131	429
12	CH_3CH_2	Cl	$CH_3CH(OH)$	0.03	0.005	2.6/18	−5.0	1000	131	429
13	CH_3CH_2	Cl	$(CH_3)_3C$	0.02	0.01	7.3/12.2	−5.3	5	111	441

[a]Inhibition of AVP8 and AVP5 in an FLT assay using Ac-WLRGG*ARC(PT14)-NH_2 as substrate. Data represent mean of at least 2 experiments performed in duplicate. Individual data points in each experiment were within 2-fold range with each other. [b]High throughput equilibrium solubility at pH 6.8. [c]Molecular weight. [d]Not determined. [e]Racemic.

the nonprime site and all amide groups of the inhibitor are involved in hydrogen bonding interactions with the protease. While no specific interaction with the protein is apparent for the P3 phenyl group of **1**, the P4 chlorophenyl moiety nicely fills the hydrophobic S4 pocket of the substrate binding site and is involved in a cation−π interaction with the side chain of Arg48. The structure also reveals a halogen bonding interaction from the 3-chloro substituent of the P4 phenyl ring to the Ala46 backbone carbonyl oxygen. The chlorine to carbonyl oxygen distance is 3.1 Å in agreement with the optimal calculated interaction distance of 312 pm.[14]

For inhibitor **2**, the thioimidate moiety resulting from attack of the Cys122 SH-group on the nitrile group of the inhibitor forms a hydrogen bond with Gln115; this is the only hydrogen bond interaction inhibitor **2** engages in (Figure 2B). Unlike inhibitor **1**, compound **2** does not extend into the substrate binding pocket.

Unfortunately, despite the high potency of inhibitor **1** in the biochemical assay, the compound was not active in a viral replication assay. We attributed this observation to the poor permeability of **1**, due to its peptidic nature. On the basis of the available structural information, we thus elaborated an optimization strategy toward inhibitors with improved permeability, with the reduction of polar surface area (PSA) and MW of the original hit **1** as the key objective. In a first step, we focused on the modification of the P4 subsite, and the results of these investigations are summarized in Table 1 (compounds **3**–**6**). Compound **3**, which lacks the methylsulfonyl amino group present in **1**, was only 10-fold less potent than the latter. This is in line with the fact that the X-ray structure of **1** suggested that the sulfonamide moiety does not contribute to binding significantly. Attaching a small substituent, such as a hydroxyl group, at the 2-position of the P4 chlorophenylacetyl moiety in **3** (compound **4**) restored the original activity. Further analysis of the X-ray structure suggested that the hydrophobic interactions within the lipophilic S4 pocket could be further increased by attaching an additional substituent at the 5-position of the phenyl ring. We explored several substituents at this position, and the 3,5-dichloro substitution pattern proved to be optimal, resulting in

dx.doi.org/10.1021/ml500224t | ACS Med. Chem. Lett. 2014, 5, 937−941

a 70 nM inhibitor (compound **5**). Finally, incorporating a methyl substituent at the 2-position of the 3,5-dichlorophenyl moiety resulted in compound **6**, which exhibited an IC_{50} of 30 nM. Compounds **4**−**6** are equipotent with **1** as enzyme inhibitors, but have a significantly reduced MW and PSA. Unfortunately, these features did not translate into improved permeability compared with **1**, as compounds **3** and **5** were found to have low passive permeability in a Caco-2 assay and low permeability in the Pampa assay.[15,16]

In a next step we addressed the impact of modifications of the P3 residue. This included replacement of the benzyl moiety in inhibitor **5** by a 2-methylpyridinyl, an aminomethyl, a 1-hydroxyethyl, or a *tert*-butyl residue. The incorporation of 2-pyridinyl alanine in P3 (Table 1, compound **7**) was designed to establish an intramolecular hydrogen bond to the P2/P3 amide group;[17] however, **7** displayed only moderate potency. Polar P3 groups, as in compounds **8** and **9**, as well as lipophilic residues, as in **10**, maintained the activity. For compound **10** the presence of a lipophilic *tert*-butyl residue in P3 also resulted in slightly improved permeability in the Caco-2 assay, compared to **5**. We were able to obtain an X-ray cocrystal stucture of glycine nitrile derivative **9** bound to AVP8, which showed that the binding mode of **9** is identical to that of **1** (Figure 3). As predicted, the 3,5-dichlorophenyl group nicely fills the S4 subsite.

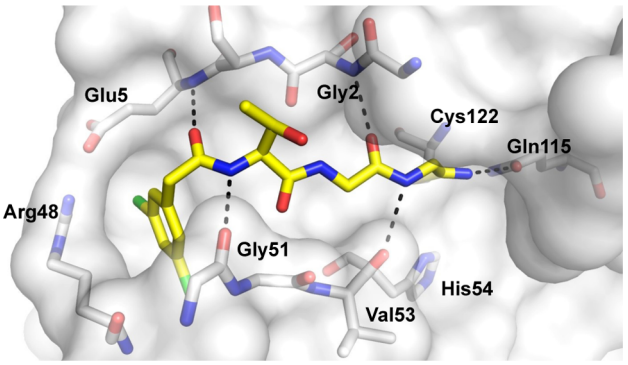

Figure 3. X-ray structure of inhibitor **9** (PDB code 4PIQ) in AVP8. The picture was produced using PyMol.

The results obtained for derivatives of **1** with modifications either in P3 or P4 subsequently led to the design of compounds incorporating small polar or lipophilic substituents at the 2-position of the P4 moiety and amino acids with branched side chains in P3 (compounds **11**−**13**). Compounds **12** and **13**, which both incorporate an ethyl substituent at the 2-position of the P4 subunit, showed a small improvement in potency relative to the corresponding unsubstituted parent compounds **9** and **10**, respectively. Evaluation of compounds **7**−**13** in the Caco-2 assay revealed slightly improved passive permeability for the *t*-butyl glycine-containing inhibitors **10** and **13**. However, all of the glycine nitrile derivatives investigated displayed a high efflux ratio.

In line with the low to moderate permeability of the various glycine nitrile-based inhibitors derived from **1**, a substantial potency shift was observed between the biochemical FLT assay[18] and the cellular viral cytopathic effect (CPE) assay. For example, while compound **13** inhibits AVP8 and AVP5 with IC_{50} values of 20 and 10 nM, respectively, it displayed an EC_{50} of only 2.5 μM in the CPE assay in HEK293 cells.

It became evident that for further improvement of permeability and cellular potency a replacement of at least one amide bond would be indispensable. One possibility to achieve this was to merge the peptidic series with the pyrimidine nitrile **2**, such that the pyrimidine core would serve as a surrogate for the P1/P2 amide bond. The cocrystal structure of **2** suggested that for this type of inhibitors the attachment point for the P2−P4 substituent would need to be shifted from the 5 to the 4 position of the pyrimidine ring, in order to enable extension of the pyrimidine template into the active site. In addition, molecular modeling predicted an aminomethyl linker group as the most promising vector to expand from the 4 position of the pyrimidine ring into the substrate binding pocket. The results and the profiling data obtained with hybrid inhibitors originating from the peptidic scaffold and the pyrimidine nitrile scaffold are summarized in Table 2. Generally, replacement of the glycine nitrile part of type **1** inhibitors by a pyrimidine nitrile moiety resulted in increased potency. At the same time and very importantly, inhibitors **14**−**17** exhibited the hoped-for-shift toward higher permeability. They displayed high permeability and a passive trans-cellular transport mechanism in the Caco-2 assay, thus demonstrating that the replacement of one amide bond indeed resulted in greatly improved permeability. It is noteworthy that inhibitors **14**−**17** in addition no longer displayed efflux. Interestingly, compared to the corresponding glycine nitrile derivative **12**, pyrimidine nitrile **17**, which lacks a 2 substituent on the aromatic P4 moiety (i.e., R1 = H, Table 2) displays

Table 2. Results and Profiling Data of Pyrimidine Nitriles 14−17

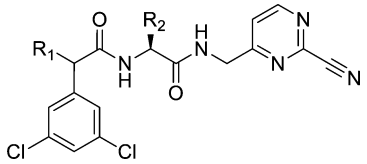

compd	R1	R2	IC_{50} AVP8[a] (μM)	IC_{50} AVP5[a] (μM)	EC_{50} CPE[b] (μM)	Caco-2 (A_B)/(B−A) (10^{-6} cm/s)	log Pampa (10^{-6} cm/s)	Sol[c] (μM)	PSA (Å^2)	MW
14	$(CH_3)_2N$[d]	$CH_3CH_2CH(CH_3)$	0.06	0.02	6.7	17.8/10.1	−3.8	61	111	477
15	OH[e]	$CH_3CH_2CH(CH_3)$	0.02	0.008	7.2	18.3/11.3	−5.3	236	128	450
16	H	CH_3OCH_2	0.004	0.002	3.2	23.2/14.8	−4.9	52	117	422
17	H	$CH_3CH(OH)$	0.003	0.002	1.2	12.2/14.1	−5.4	556	128	422

[a]Inhibition of AVP8 and AVP5 in an FLT assay using Ac-WLRGG*ARC(PT14)-NH2 as substrate. Data represent the mean of at least 2 experiments performed in duplicate. [b]HEK293 cells; EC_{50} data represent the mean of at least 5 independent assays. [c]High throughput equilibrium solubility at pH 6.8. [d]Racemic. [e]*S*-enantiomer.

dx.doi.org/10.1021/ml500224t | *ACS Med. Chem. Lett.* 2014, 5, 937−941

significantly higher potency. Compound **17** exhibits a single digit nanomolar IC_{50} in the biochemical assays, which makes **16** and **17** the most potent inhibitors identified from this work. Unfortunately, however, despite their drug-like properties, **16** and **17** displayed EC_{50}s of only 3 and 1 μM, respectively, in the CPE assay. The reasons for this moderate cellular activity remain to be elucidated.

All pyrimidine nitrile inhibitors showed excellent specificity toward a panel of five human cysteine proteases; these data are summarized in the Supporting Information.

Figure 4 displays the X-ray cocrystal structure of **14** with adenain, which provides experimental confirmation of the predicted binding mode of the designed hybrid inhibitors, **14**–**17**. Thus, as illustrated in Figure 4 by the superposition of **14** and **2**, the shift of the pyrimidine substituent from the 5- to the 4-position directed the attached P2–P4 subunit into the substrate binding site.

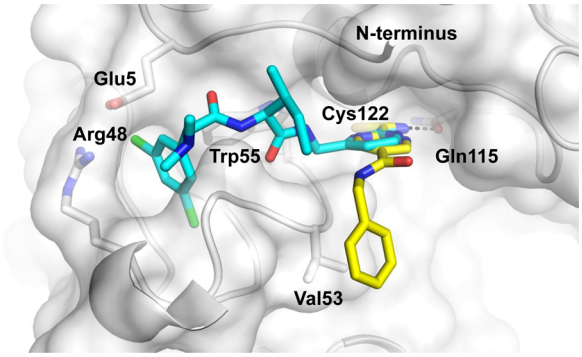

Figure 4. Superposition of X-ray structures of inhibitor **14** (cyan, PDB code 4PIS) and **2** (yellow, PDB code 4PID). The picture was produced using PyMol.

For the preparation of the glycine nitrile derivatives **4**, **7**–**10**, **12**, and **13**, a mixed solid phase/solution synthesis strategy was used as summarized in Scheme 1 for inhibitor **10**. The solid phase part of the synthesis was performed on a trityl-based polystyrene resin. Coupling reactions were carried out under Fmoc-based solid phase peptide synthesis conditions.[19] Capped dipeptide **21** was cleaved from the resin under mild acidic conditions (HFIP), and the synthesis of **10** was completed by coupling intermediate **22** with aminoacetonitrile. Glycine nitrile-based inhibitors **1**, **3**, **5**, **6**, and **11** were prepared in solution.

The synthesis of the pyrimidine nitriles listed in Table 2 followed the route exemplified in Scheme 2 for compound **16**.

Scheme 1[a]

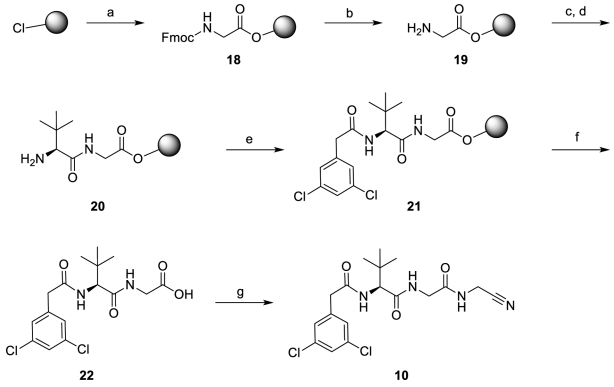

[a]Reagents and conditions. (a) Fmoc-Gly-OH, DIEA, CH_2Cl_2; (b) piperidine, DMA; (c) Fmoc-L-*α*-*tert*-butyl-glycine, TBTU, DIEA, NMP; (d) 4-methylpiperidine, DMA; (e) 2-(3,5-dichlorophenyl)acetic acid, TBTU, DIEA, NMP; (f) HFIP, CH_2Cl_2; (g) aminoacetonitrile, TBTU, DIEA, DMF.

Scheme 2[a]

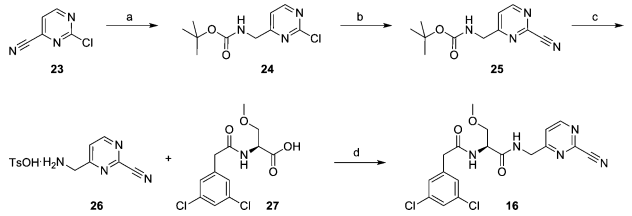

[a]Reagents and conditions. (a) H_2, 5% $Rh(Al_2O_3)$, iPrOAc, BOC_2O, 62%; (b) NaCN, DABCO, DMSO, 97%; (c) TsOH, CH_3CN, 95%; (d) PyBOP, *N*-methylmorpholine, DMF, 64%.

Reduction of the cyano group of commercially available 2-chloropyrimidine-4-carbonitrile (**23**) with hydrogen gas and $Rh(Al_2O_3)$ afforded the corresponding amine, which was Boc-protected in situ. Intermediate **25** was obtained by the displacement of the 2-chloro substituent with cyanide ion. The Boc protecting group was removed with *p*-toluenesulfonic acid in acetonitrile to produce amine **26**. Subsequent PyBOP-mediated coupling of **27** and **26** yielded the target molecule **16**.

In summary, starting from a peptide nitrile (**1**) and a pyrimidine nitrile fragment (**2**) we have discovered a new class of highly potent adenain inhibitors. High-resolution X-ray cocrystal structures of **1** and **2** enabled rapid structure-guided optimization and provided the basis for a merger of the two initial starting points. Our medicinal chemistry strategy resulted in highly potent inhibitors of adenain with high permeability and good solubility. X-ray cocrystal stuctures of optimized inhibitors confirmed the predicted binding mode and provided valuable information for the design of new nonpeptidic inhibitors. Pyrimidine nitrile inhibitors **16** and **17** represent excellent lead compounds with drug-like properties suitable for further optimization of cellular potency. These efforts will be addressed in a subsequent manuscript.

■ ASSOCIATED CONTENT

Supporting Information

Description of the inhibition assays; experimental procedures for the synthesis and characterization (^{1}H NMR and HR-MS) of compounds **1**–**17**. Inhibition data for antitargets for compounds **13**–**17**. The atomic coordinates and structure factors for the X-ray crystal structures of adenain in complex with **1**, **2**, **9**, and **14** have been deposited in the Protein Data Bank RSCB PDB. This material is available free of charge via the Internet at http://pubs.acs.org.

■ AUTHOR INFORMATION

Corresponding Author

*(E.A.) Phone: + 41 61 696 1227. E-mail: eva.altmann@novartis.com.

Notes

The authors declare no competing financial interest.

■ ACKNOWLEDGMENTS

The authors thank Estelle Ngo, Raphael Gattlen, and Mina Aikawa for excellent technical assistance.

■ ABBREVIATIONS

AVP2, adenovirus protease serotype 2; AVP5, adenovirus protease serotype 5; AVP8, adenovirus protease serotype 8; BOC2O, di-*tert*-butyldicarbonat; CPE, cytopathic effect; DABCO, 1,4-diazabicyclo[2.2.2] octane; DIEA, *N*,*N*-diisopropylethylamine; DMA, *N*,*N*-dimethylacetamide; DMSO, dimethyl sulfoxide; FLT, fluorescence lifetime; HFIP, 1,1,1,3,3,3-hexafluoro-2-propanol; NMP, 1-methyl-2-pyrrolidinone; PSA, polar surface area; PyBOP, benzotriazol-yloxytripyrrolidinophosphoniumhexafluorophosphate; TBTU, *O*-(benzotriazol-1-yl) -*N*,*N*,*N*′,*N*′-tetramethyl-uronium tetrafluoroborate

■ REFERENCES

(1) Lenaerts, L.; De Clercq, E.; Naesens, L. Clinical features and treatment of adenovirus infections. *Rev. Med. Virol.* **2008**, *18*, 357−374.
(2) Kaufman, H. E. Adenovirus advances: new diagnostic and therapeutic options. *Curr. Opin. Ophthalmol.* **2011**, *22*, 290−293.
(3) Kinchington, P. R.; Romanowski, E. G.; Gordon, Y. J. Prospects for adenoviral antivirals. *J. Antimicrob. Chemother.* **2005**, *55*, 424−429.
(4) Zhou, X.; Robinson, C. M.; Rajaiya, J.; Seto, D.; Jones, M. S.; Dyer, D. W.; Chodosh, J. Analysis of human adenovirus type 19 associated with epidemic keratoconjunctivitis and its reclassification as adenovirus type 64. *Invest. Ophthalmol. Vis. Sci.* **2012**, *53*, 2804−2811.
(5) Pihos, A. M. Epdidemic keratoconjunctivitis: A review of current concepts in management. *J. Optom.* **2013**, *6*, 69−74.
(6) Weber, J. M. Adenain the adenovirus endoprotease. *Acta Microbiol. Immunol. Hung.* **2003**, *50*, 95−101.
(7) McGrath, W. J.; Baniecki, M. L.; Peters, E.; Green, D. T. Mangel, W.F. Roles of two conserved cysteine residues in the activation of human adenovirus proteinase. *Biochem.* **2001**, *40*, 14468−14474.
(8) Greber, U. F. Virus assembly and disassembly: the adenovirus as a trigger factor. *Rev. Med. Virol.* **1998**, *8*, 213−222.
(9) Greber, U. F.; Webster, P.; Weber, J.; Helenius, A. The role of adenovirus protease in virus entry into cells. *EMBO J.* **1996**, *15*, 1766−1777.
(10) Chen, P. H.; Ornelles, D. A.; Shenk, T. The adenovirus L3 23-kilodalton proteinase cleaves the amino-terminal head domain from cytokeratin 18 and disrupts the cytokeratin network of HeLa cells. *J. Virol.* **1993**, *67*, 3507−3514.
(11) Mangel, W. F.; Banjecki, M. L.; McGrath, W. J. Specific interactions of the adenovirus proteinase with the viral DNA, an 11-amino acid viral peptide, and the cellular protein actin. *Cell. Mol. Life Sci.* **2003**, *60*, 2347−2355.
(12) The paper describes weak, non-drug like compounds with unknown binding mode. McGrath, W. J.; Graziano, V.; Zabrocka, K.; Mangel, W. F. First generation inhibitors of the adenovirus proteinase. *FEBS Lett.* **2013**, *587*, 2332−2339.
(13) Ruzindana-Umunyana, A.; Imbeault, L.; Weber, J. M. Substrate specificity of adenovirus. *Virus Res.* **2002**, *89*, 41−52.
(14) Wilcken, R.; Zimmermann, M. O.; Lange, A.; Zahn, S.; Boeckler, F. M. Using halogen bonds to address the protein backbone: a systematic evaluation. *J. Comput-Aided Mol. Des.* **2012**, *26*, 935−945.
(15) Faller, B. Artificial membrane assays to assess permeability. *Curr. Drug Metab.* **2008**, *9*, 886−892.
(16) Van Breemen, R. B.; Li, Y. Caco-2 cell permeability to measure drug absorption. *Expert Opin. Drug Metab. Toxicol.* **2005**, *1*, 175−185.
(17) Kuhn, B.; Mohr, P.; Stahl, M. Intramolecular hydrogen bonding in medicinal chemistry. *J. Med. Chem.* **2010**, *53*, 2601−2611.
(18) Boettcher, A.; Gradoux, N.; Lorthiois, E.; Brandl, T.; Orain, D.; Schiering, N.; Cumin, F.; Woelcke, J.; Hassiepen, U. Fluorescence lifetime-based competitive binding assay for measuring the binding potency of protease inhibitors in vitro. *J. Biomol. Screening* **2014**, *19*, 870−878.
(19) Gongora-Benitez, M.; Tulla-Puche, J.; Albericio, F. Handles for Fmoc solid-phase synthesis of protected peptides. *ACS Comb. Sci.* **2013**, *15*, 217−228.